

Spatial Resolution of an Inorganic Crystal-Based Hard X-Ray Imager

Chen Hu¹, Member, IEEE, Liyuan Zhang, Member, IEEE, Ren-Yuan Zhu¹, Senior Member, IEEE, Junfeng Chen, Member, IEEE, Dongzhou Ding, Yu Wang, and Mingrong Zhang

Abstract—Gigahertz hard X-ray imaging presents an unprecedented challenge to both timing and spatial resolutions for inorganic scintillator-based front imagers. A beam test with 30-keV X-rays from the Advanced Photon Source (APS) showed that 5-mm BaF₂ plates resolve well 30-keV X-ray septuplets of 27-ps width and 2.83-ns spacing. Pixelated crystal screens with a pitch down to 400 μm were fabricated by mechanic slicing for BaF₂, BaF₂:Y, and LYSO crystals. Their spatial resolution and detection efficiency for hard X-rays are defined by the pitch and thickness, respectively. Thicker monolithic crystal screens show poorer spatial resolution, which may be improved using a small optical aperture with a loss in both efficiency and dynamic range for hard X-rays. Future plans include pursuing smaller crystal pitches by laser slicing and research and development on novel ultrafast inorganic scintillators.

Index Terms—Barium fluoride, LYSO, spatial resolution, ultrafast, X-ray imaging.

I. INTRODUCTION

INSPIRED by total absorption crystal calorimetry in high energy physics (HEP), a pixelated ultrafast inorganic scintillator-based front imager was proposed for Gigahertz (GHz) hard X-ray imaging [1]–[4] to study the dynamics of material evolution related to the nuclear Big Bang [1]. Such an imager features a subnanosecond (ns) scintillation pulsewidth to cope with the unprecedented short bunch spacing and total X-ray absorption to take full advantage of the dynamic range offered by the high-intensity X-ray pulses. Fig. 1 shows a schematic of the imager concept with a pixelated ultrafast scintillator screen, a pixelated ultrafast photodetector, and ultrafast readout electronics [1].

Two types of imagers (Types I and II) require 2 ns and 300 ps frame rates, respectively, for X-rays up to 30 and

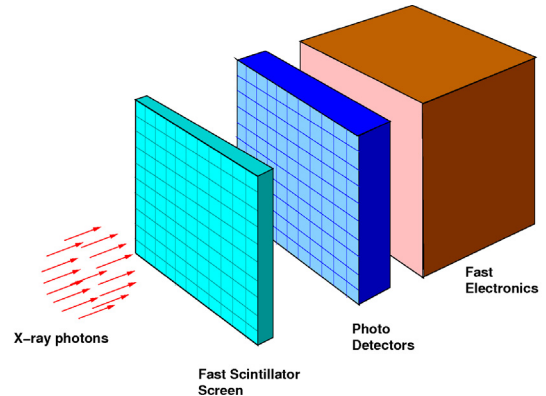


Fig. 1. Schematic showing a pixelated ultrafast inorganic scintillator-based front imager concept for GHz hard X-ray imaging.

126 keV [1]. Measurements of the temporal response of a prototype imager were carried out at both the Caltech Crystal Lab and the Advanced Photon Source (APS) facility for a dozen different fast and ultrafast crystal scintillators [2]–[4]. Their scintillation performance is listed in Table I. As shown in the table, with 0.5 ns decay time, BaF₂ provides a high light output in the first ns and a good efficiency for hard X-rays from 30 to 126 keV. Fig. 2 shows the pulse shape measured by a Hamamatsu Photomultiplier Tube (PMT) R2059 (top) and a Photech MCP-PMT240 (bottom), respectively, for a BaF₂ crystal excited by ²²Na γ-rays. A decay time of 0.5 ns was clearly observed using the Photech Microchannel Plate-Photomultiplier Tube (MCP-PMT). We also notice small access, indicating a faster decay component, which was also reported in [5].

Ultrafast inorganic scintillators, such as BaF₂ and BaF₂:Y, resolve X-ray bunches for continuous eight septuplet bunches of 27-ps width and 2.83-ns bunch spacing, providing a proof of principle for an ultrafast inorganic scintillator-based total absorption front imager for GHz hard X-ray imaging [2]–[4]. Fig. 3 shows an example of the time-resolved X-ray pulses with 2.83-ns bunch spacing observed with a BaF₂ screen. However, BaF₂ also has a slow scintillation component with a 600 ns decay time which causes pile-up. Yttrium doping in BaF₂ suppresses its slow scintillation light significantly while maintaining its ultrafast scintillation light [3], [6].

This article discusses the spatial resolution for an ultrafast inorganic scintillator-based X-ray imager. BaF₂ and BaF₂:Y crystal screens were produced by the Beijing Glass Research Institute (BGRI) and the Shanghai Institute of Ceramics (SIC),

Manuscript received November 15, 2019; revised January 30, 2020; accepted February 20, 2020. Date of publication March 5, 2020; date of current version June 19, 2020. This work was supported in part by the U.S. Department of Energy, Office of High Energy Physics Program under Award DE-SC0011925 and in part by the National Natural Science Funds of China under Grant 51402332 and Grant 11475241.

Chen Hu, Liyuan Zhang, and Ren-Yuan Zhu are with HEP, California Institute of Technology, Pasadena, CA 91125 USA (e-mail: zhu@hep.caltech.edu).

Junfeng Chen and Dongzhou Ding are with the Research and Development Center, Shanghai Institute of Ceramics, Chinese Academy of Sciences, Shanghai 201899, China.

Yu Wang is with Sichuan Tianle Photonics Company, Ltd, Chengdu 611200, China.

Mingrong Zhang is with the Beijing Glass Research Institute, Beijing 101111, China.

Color versions of one or more of the figures in this article are available online at <http://ieeexplore.ieee.org>.

Digital Object Identifier 10.1109/TNS.2020.2978800

TABLE I
CANDIDATE SCINTILLATORS FOR GHZ HARD X-RAY IMAGING TESTED AT APS

	BaF ₂	BaF ₂ (:Y)	ZnO (:Ga)	YAP (:Yb)	YAG (:Yb)	β- Ga ₂ O ₃	LYSO (:Ce)	LuAG (:Ce)	YAP (:Ce)	GAGG (:Ce)	LuYAP (:Ce)	YSO (:Ce)
Density (g/cm ³)	4.89	4.89	5.67	5.35	4.56	5.94	7.4	6.76	5.35	6.5	7.2 ^f	4.44
Melting Points (°C)	1280	1280	1975	1870	1940	1725	2050	2060	1870	1850	1930	2070
X ₀ (cm)	2.03	2.03	2.51	2.77	3.53	2.51	1.14	1.45	2.77	1.63	1.37	3.10
R _M (cm)	3.1	3.1	2.28	2.4	2.76	2.20	2.07	2.15	2.4	2.20	2.01	2.93
λ _i (cm)	30.7	30.7	22.2	22.4	25.2	20.9	20.9	20.6	22.4	21.5	19.5	27.8
Z _{eff}	51.6	51.6	27.7	31.9	30	28.1	64.8	60.3	31.9	51.8	58.6	33.3
dE/dX (MeV/cm)	6.52	6.52	8.42	8.05	7.01	8.82	9.55	9.22	8.05	8.96	9.82	6.57
λ _{peak} ^a (nm)	300 220	300 220	380	350	350	380	420	520	370	540	385	420
Refractive Index ^b	1.50	1.50	2.1	1.96	1.87	1.97	1.82	1.84	1.96	1.92	1.94	1.78
Normalized Light Yield ^{a,c}	42 4.8	1.7 4.8	6.6 ^d	0.19 ^d	0.36 ^d	6.5 0.5	100	35 ^e 48 ^e	9 32	115	16 15	80
Total Light Yield (ph/MeV)	13,000	2,000	2,000 ^d	57 ^d	110 ^d	2,100	30,000	25,000 ^e	12,000	34,400	10,000	24,000
Decay Time ^a (ns)	600 0.5	600 0.5	<1	1.5	4	148 6	40	820 50	191 25	53	1485 36	75
Light Yield in 1 st ns (photons/MeV)	1200	1200	610 ^d	28 ^d	24 ^d	43	740	240	391	640	125	318
40 keV Att. Length (λ) (1/e, mm)	0.106	0.106	0.407	0.314	0.439	0.394	0.185	0.251	0.314	0.319	0.214	0.334

^aTop line: slow component, bottom line: fast component.

^bAt the wavelength of the emission maximum.

^cExcited by Gamma rays.

^dExcited by Alpha particles.

^eCeramic with 0.3 Mg at% co-doping.

^fBased on Lu_{0.7}Y_{0.3}AlO₃:Ce.

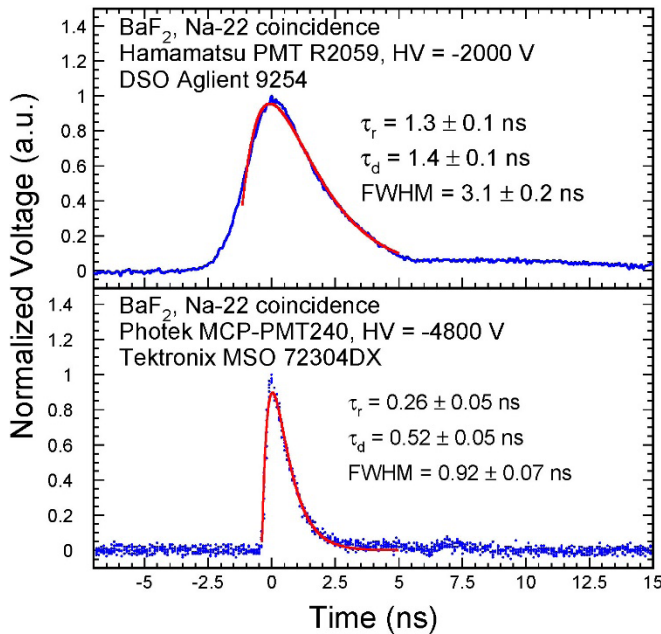


Fig. 2. Normalized pulse shape for the BaF₂ samples excited by ²²Na γ-rays, measured with a Hamamatsu PMT R2059 (top) and a Photek MCP-PMT240 (bottom), respectively.

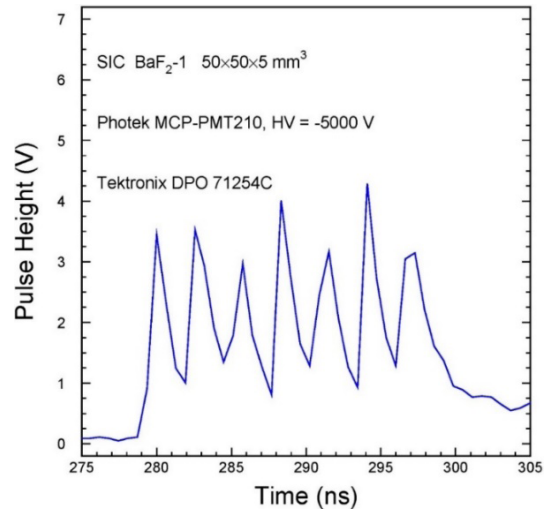


Fig. 3. BaF₂ imaging for 2.83-ns bunch spacing.

respectively. LYSO:Ce crystal screens were produced by SIC and Sichuan Tianle Photonics Company, Ltd. Pixelated crystal screens with a pitch down to 400 μm were fabricated by

mechanic slicing. X-ray images of these pixelated screens were taken using commercial cameras. The spatial resolution of monolithic crystal screens was also measured with charge-coupled device (CCD) cameras. The effects of the sample thickness and an optical aperture on spatial resolution are also discussed.

TABLE II
BASIC PROPERTIES FOR THE PIXELATED CRYSTAL SCREENS INVESTIGATED IN THIS ARTICLE

Crystal	Dimension (mm ³)	Pitch (mm)	Gap (mm)	Depth (mm)	Reflector	# of wrapped faces	Vendor	# of λ (40 keV X-ray)	# of samples
LYSO:Ce	20×20×1	0.40	0.12	0.7	TiO ₂	4	SIC	5.4	2
LYSO:Ce	20×20×1	0.828	0.08	1.0	ESR	4	Tianle	5.4	6
BaF ₂	20×20×5	0.98	0.18	4.0	TiO ₂	5	BGRI	47.2	1
BaF ₂ :Y	20×20×5	0.98	0.18	4.5	BaSO ₄	4	SIC	47.2	1

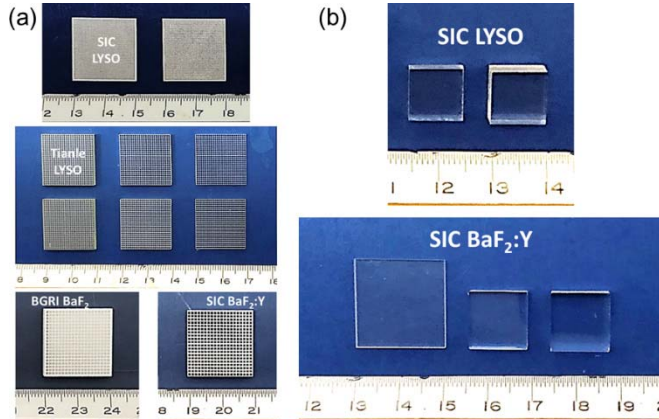


Fig. 4. (a) Photos of two pixelated LYSO from SIC (top), six pixelated LYSO from Tianle (middle), pixelated BaF₂ and BaF₂:Y crystal screens from BGRI and SIC, respectively (bottom). (b) Photos of two SIC LYSO crystal of 10×10×3 mm³ and 10×10×5 mm³ placed from left to right (top), and three SIC BaF₂:Y crystal of 20×20×1.5 mm³, 13×13×3 mm³, and 13×13×5 mm³ placed from left to right (bottom).

TABLE III
BASIC PROPERTIES FOR THE MONOLITHIC CRYSTAL SCREENS

Crystal	Dimension (mm ³)	Vendor	# of λ (40 keV X-ray)	# of Samples
LYSO:Ce	10×10×3	SIC	16.2	1
LYSO:Ce	10×10×5	SIC	27.0	1
BaF ₂ :Y	20×20×1.5	SIC	14.1	1
BaF ₂ :Y	13×13×3	SIC	28.3	1
BaF ₂ :Y	13×13×5	SIC	47.2	1

II. SAMPLES AND EXPERIMENTAL DETAILS

Fig. 4(a) shows pixelated LYSO, BaF₂, and BaF₂:Y crystal screens from various vendors. They were cut and polished, before mechanical slicing, into various crystal pitches. Crystal pitches down to 400 μ m were obtained by mechanical dicing. It is also known that crystal pitches down to 25 μ m may be obtained by laser slicing [7]. Reflectors and glues were used to fill in the gaps. While all samples except the BGRI BaF₂ had two large faces unwrapped, the BGRI BaF₂ had only one large face unwrapped. For LYSO and BaF₂:Y crystals from SIC, the one large face mechanically sliced is the front face, while the other large face is the back face. The front faces were placed facing toward the CCD cameras in our investigation. The detailed description of the pixelated crystal screens, including glue and reflectors, are listed in Table II.

Fig. 4(b) shows monolithic crystal screens of LYSO and BaF₂:Y produced by SIC. All of these samples were cut with all faces polished. Detailed information for the monolithic crystal screens is listed in Table III.

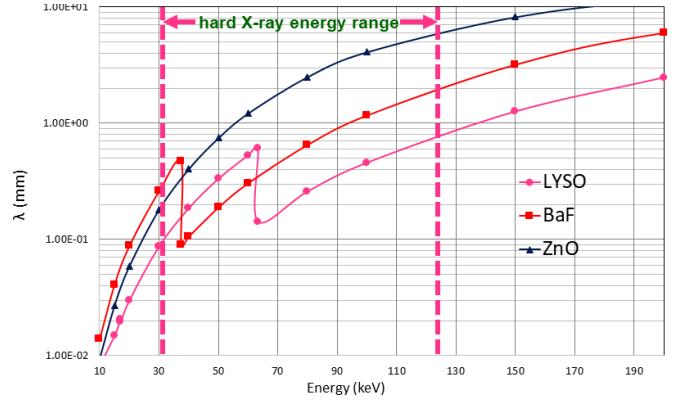


Fig. 5. X-ray attenuation length is shown as a function of energy for LYSO (red dots), BaF₂ (red squares) and ZnO (blue triangles), respectively.

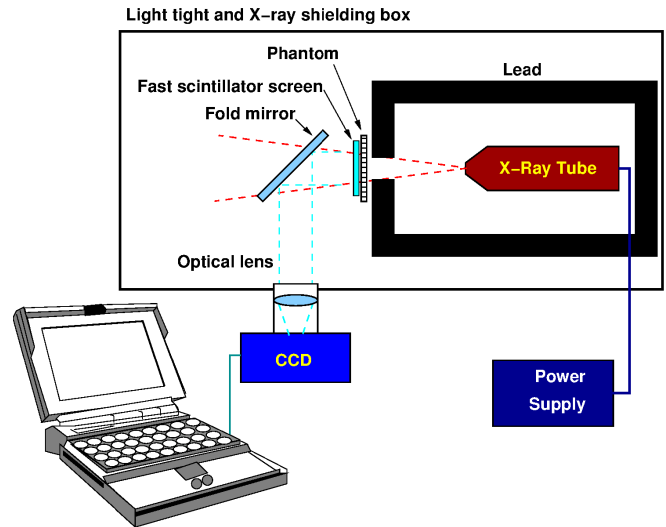


Fig. 6. Schematic for X-ray imaging setup of pixelated and monolithic crystal screens measured by PCO and Princeton CCD cameras for \sim 8-keV X-rays from an Amptek Eclipse-III tube.

Fig. 5 shows the X-ray attenuation length as a function of X-ray energy for LYSO, BaF₂, and ZnO, calculated according to the National Institute of Standards and Technology (NIST) data [8]. For hard X-rays of 100 keV [1], the X-ray attenuation length is 0.4, 1, and 4 mm for LYSO, BaF₂, and ZnO, respectively. Five attenuation lengths are required for the proposed total absorption concept, corresponding to 2, 5, and 20 mm for LYSO, BaF₂, and ZnO, respectively.

Fig. 6 is a schematic showing the X-ray imaging setup with the CCD cameras. The samples were placed in a light-tight

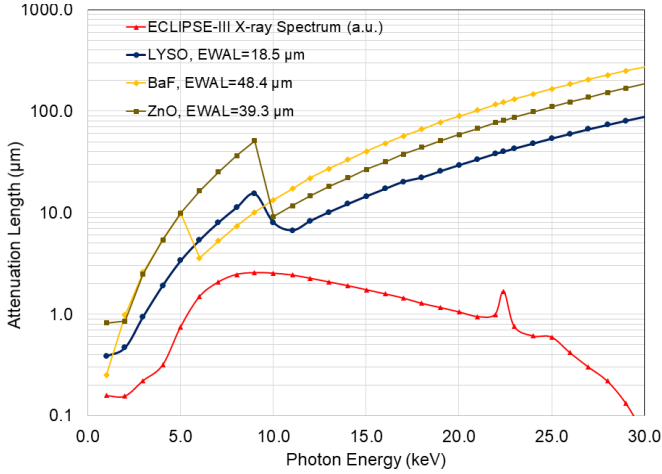


Fig. 7. X-ray emission from the Amptek Eclipse-III X-ray tube (red triangles) and attenuation lengths are shown as a function of wavelength for LYSO (blue dots), BaF₂ (yellow diamonds) and ZnO (green squares).

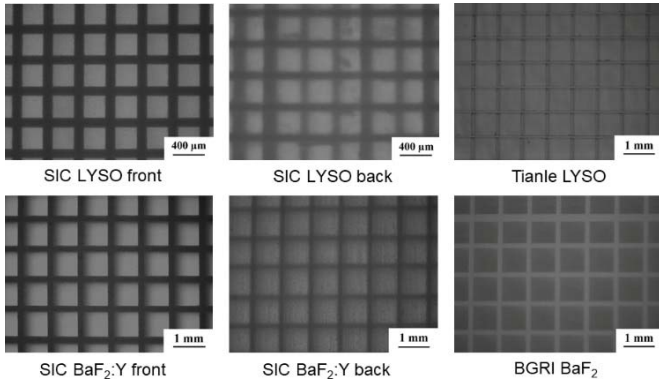


Fig. 8. Photos of the pixelated crystal screens taken by a microscope with a white LED as light source.

box with X-ray shielding and a lead line-pair pattern with five black and white line-pairs was used as a phantom. Two CCD cameras, a PCO.edge 4.2 bi and a Princeton Kuro10208, were used along with a $\Phi 25$ -mm optical lens, focusing on the crystal surface facing the CCD camera to imitating the total absorption concept.

Fig. 7 shows the emission spectrum for the X-rays generated by an Amptek Eclipse-III X-ray tube used in our investigation. The emission peak is about 8 keV with an operating voltage of 30 keV. Also shown in the figure are the attenuation lengths of LYSO, BaF₂, and ZnO based on Lawrence Berkeley National Laboratory (LBNL) data [9]. The emission-weighted attenuation length (EWAL) is defined as

$$EWAL = \frac{\int L(\lambda) Em(\lambda) d\lambda}{\int Em(\lambda) d\lambda} \quad (1)$$

where $L(\lambda)$ and $Em(\lambda)$ are the attenuation length and emission spectra. The numerical value of EWAL represents the attenuation length over the entire emission spectrum for the X-ray source used in this investigation. They are 18.5, 48.4, and 39.3 μm , respectively, for LYSO, BaF₂, and ZnO.

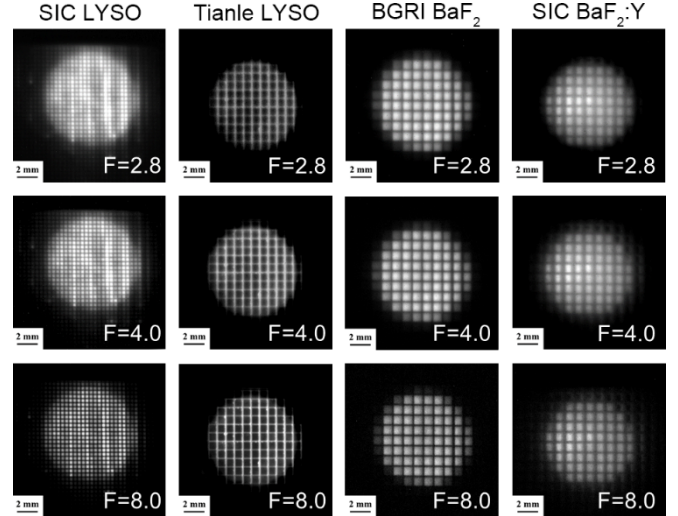


Fig. 9. X-ray images of crystal screens by PCO Camera under different apertures.

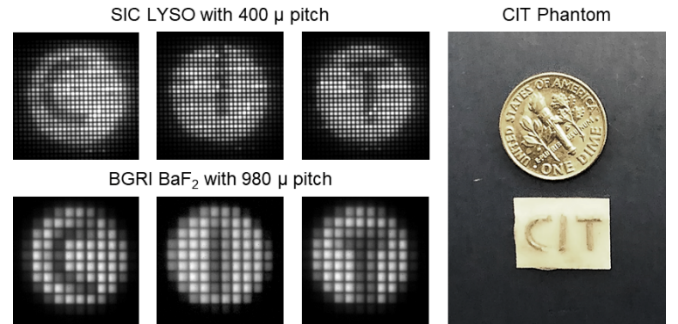


Fig. 10. X-ray Images of SIC LYSO (top) and BGRI BaF₂ (bottom) crystal screens by PCO Camera for a stainless steel wire phantom showing “CIT.”

III. RESULTS AND DISCUSSION

A. Optical and X-Ray Imaging of Pixelated Crystal Screens

Fig. 8 shows photos of the pixelated crystal screens taken with a microscope using a white LED as the light source. Photos of both the front and back faces were taken for the SIC crystal screens, because, as shown in Table II, these crystal screens were not cut-through and both large faces were not wrapped. As shown in Fig. 8, the crystal pitches and gaps can be well resolved for all crystal screens.

Fig. 9 shows the X-ray images of crystal screens taken with the PCO camera with apertures of 2.8, 4.0, and 8.0. The images taken with smaller apertures show better imaging quality. The crystal pitches of 400, 828, 980, and 980 μm were well resolved for the SIC LYSO, Tianle LYSO, BGRI BaF₂, and SIC BaF₂:Y, respectively. While the spatial resolution of the pixelated crystal screens is defined by the crystal pitch, the dynamic range of the imaging is defined by its thickness. We plan to produce crystal screens with smaller pitches (down to 25 μm [7]) by laser slicing.

Fig. 10 shows X-ray images of the SIC LYSO and BGRI BaF₂ crystal screens taken with the PCO camera using a stainless steel wire phantom. The letters “CIT” well resolve for both crystal screens, showing that pixelated an LYSO crystal

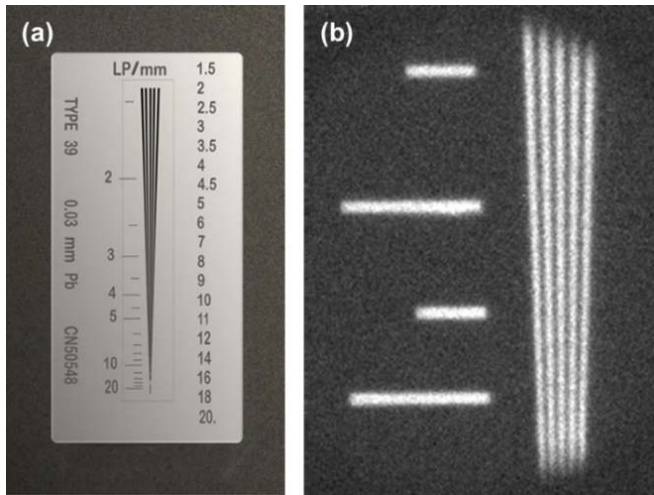


Fig. 11. Photos of line-pair pattern used as a phantom taken under (a) visible light and (b) X-ray.

with a 400- μm pitch and a BaF_2 crystal with a 980- μm pitch are capable of taking high-quality images.

B. X-Ray Imaging of Monolithic Crystal Screens

In addition to pixelated crystal screens, the spatial resolution of monolithic crystal screens was also investigated. LYSO and $\text{BaF}_2:\text{Y}$ plates from SIC were used for this investigation. The spatial resolution was measured using a line-pair pattern. Fig. 11(a) shows a standard line-pair pattern with five black and white line pairs used as a phantom. Fig. 11(b) shows the X-ray images taken with the Princeton Kuro10208 camera and the phantom located just in front of the crystal screens.

The spatial resolution of different crystal screens can be compared by using the modulation transfer function (MTF) measured at different spatial frequencies, defined as line pairs per mm (LP/mm), as shown in Fig. 11(a). The MTF is defined as

$$\text{MTF} = \frac{I_{\max} - I_{\min}}{I_{\max} + I_{\min}}. \quad (2)$$

In our case, there are five peaks and four valleys for the X-ray intensity at each spatial frequency, and the MTF value is defined by an average of the eight values for these peaks and valleys. Fig. 12 shows the MTF values as a function of the spatial frequency measured for the SIC $\text{BaF}_2:\text{Y}$ crystal screens with various thicknesses. It also shows a 5-mm thick SIC LYSO screen used as a reference. It is worthwhile noting that the spatial resolution (or MTF values) of the thicker samples is poorer (or lower), especially for the SIC $\text{BaF}_2:\text{Y}$ 5-mm sample. This is due to the fact that the soft X-rays absorbed in a few hundreds of μm so that the imaging focusing on the back surface of the screen was affected by the light propagation in the screen. Since our concept for a total absorption imager requires at least 5 and 2 mm thickness for BaF_2 and LYSO screens, respectively, for 100-keV X-rays, an improvement on spatial resolution for thicker samples is ultimately required.

One alternative approach to improve the spatial resolution for thick samples is to use a small optical aperture.

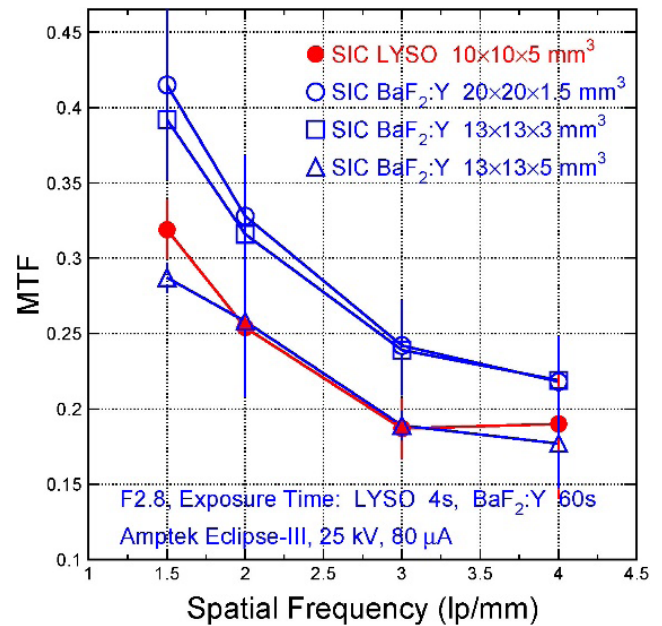


Fig. 12. MTF values obtained using the Princeton Kuro10208 camera as a function of spatial frequency for SIC $\text{BaF}_2:\text{Y}$ crystal screens with various thicknesses. A 5-mm thick SIC LYSO was used as a reference.

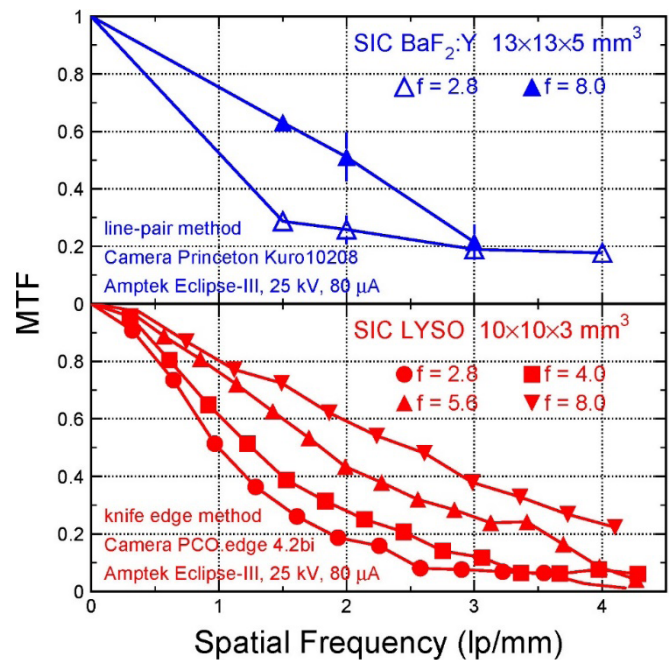


Fig. 13. MTF values as a function of spatial frequency for the $13 \times 13 \times 5 \text{ mm}^3$ SIC $\text{BaF}_2:\text{Y}$ crystal screen using the Princeton Kuro10208 camera (top) and the $10 \times 10 \times 3 \text{ mm}^3$ SIC LYSO crystal screen using the PCO.edge 4.2-bi camera (bottom) with different optical apertures.

Fig. 13 shows the MTF values as a function of spatial frequency for the $13 \times 13 \times 5 \text{ mm}^3$ SIC $\text{BaF}_2:\text{Y}$ crystal screen (top) and the $10 \times 10 \times 3 \text{ mm}^3$ SIC LYSO crystal screen (bottom) measured using the Princeton Kuro10208 camera and the PCO.edge 4.2-bi camera, respectively, with different optical apertures. While the MTF value was measured using

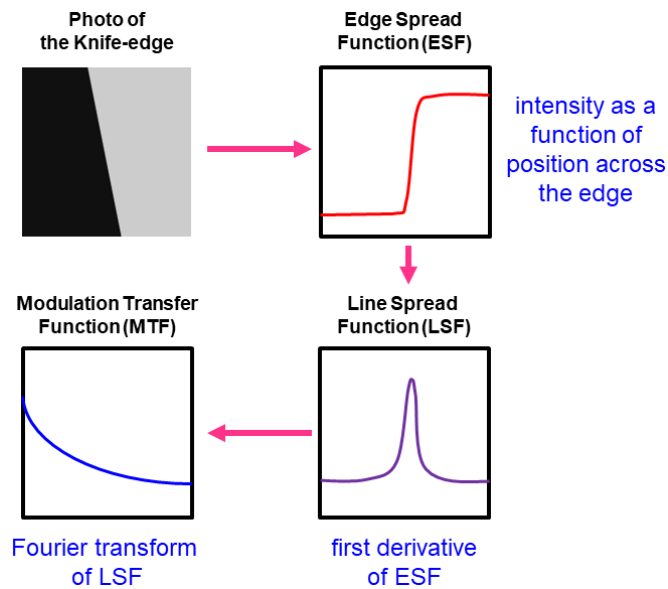


Fig. 14. Flowchart for MTF calculation by the knife-edge method.

the same method as in Fig. 12 for the SIC BaF₂ crystal, the knife-edge method was used for the LYSO crystal screen.

Fig. 14 shows a flowchart for MTF calculation using the knife-edge method. An X-ray image of a lead knife edge was taken to calculate the MTF values using a lead plate as a phantom. The X-ray intensity as a function of position across the edge was used as the edge spread function (ESF). The MTF values were calculated as the Fourier transform of the line spread function (LSF), which is the first derivative of ESF. It is interesting to note that regardless of the different methods used for the measurement, better spatial resolution can be obtained by using a smaller optical aperture, which, however, will cause a loss in both detection efficiency and dynamic range. In practice, a tradeoff between spatial resolution and dynamic range is required for an optimized imaging system.

IV. CONCLUSION

We investigated the spatial resolution of an inorganic crystal-based hard X-ray imager. Pixelated BaF₂, BaF₂:Y, and LYSO crystal screens with pitches down to 400 μm were fabricated by mechanic slicing. Optical and X-ray images were taken using a PCO camera with different optical apertures. Their spatial resolution and detection efficiency for hard X-rays are defined by the pitch and thickness, respectively.

Spatial resolution was also investigated for monolithic crystal screens. Thicker monolithic crystal screens show poorer spatial resolution, which may be improved using a smaller optical aperture with losses in both the detection efficiency and the dynamic range for hard X-rays.

We plan to pursue pixelated crystal screens with a pitch down to 25 μm by laser slicing. Additional ultrafast inorganic scintillators, such as ZnO:Ga films [4], [10] and all inorganic Cs Pb halide perovskite quantum dots [11], [12] etc., are also being considered.

ACKNOWLEDGMENT

The authors would like to thank PCO and Princeton companies for providing the charge-coupled device (CCD) cameras used in this investigation.

REFERENCES

- [1] P. Denes, S. Gruner, M. Stevens, and Z. Wang, Eds., "Ultrafast and high-energy X-ray imaging technologies and applications," Los Alamos Nat. Lab., Santa Fe, NM, USA, Tech. Rep. LA-UR-17-22085, Aug. 2016. [Online]. Available: https://www.lanl.gov/science-innovation/science-facilities/marie/_assets/docs/workshops/ultrafast-high-energy-x-ray.pdf
- [2] C. Hu *et al.*, "Ultrafast inorganic scintillators for gigahertz hard X-ray imaging," *IEEE Trans. Nucl. Sci.*, vol. 65, no. 8, pp. 2097–2104, Aug. 2018.
- [3] C. Hu *et al.*, "Ultrafast inorganic scintillator-based front imager for gigahertz hard X-ray imaging," *Nucl. Instrum. Methods Phys. Res. A, Accel., Spectrometers, Detectors Associated Equip.*, vol. 940, pp. 223–229, Oct. 2019.
- [4] C. Hu *et al.*, "BaF₂: Y and ZnO: Ga crystal scintillators for GHz hard X-ray imaging," *Nucl. Instrum. Methods Phys. Res. A, Accel., Spectrometers, Detectors Associated Equip.*, vol. 950, Jan. 2020, Art. no. 162767, doi: 10.1016/j.nima.2019.162767.
- [5] S. Gundacker *et al.*, "Experimental time resolution limits of modern SiPMs and TOF-PET detectors exploring different scintillators and Cherenkov emission," *Phys. Med. Biol.*, vol. 65, no. 2, Jan. 2020, Art. no. 025001.
- [6] C. Hu, C. Xu, L. Zhang, Q. Zhang, and R.-Y. Zhu, "Development of yttrium-doped BaF₂ crystals for future HEP experiments," *IEEE Trans. Nucl. Sci.*, vol. 66, no. 7, pp. 1854–1860, Jul. 2019.
- [7] E. Wiener-Avneer and J. E. McFall, "X-ray imaging array detector and laser micro-milling method for fabricating array," U.S. Patent 6087618 A, Jul. 11, 2000.
- [8] *NIST Online X-Ray Mass Attenuation Coefficients*. [Online]. Available: <https://physics.nist.gov/PhysRefData/XrayMassCoef/tab3.html>
- [9] *LBL Online X-Ray Attenuation Length*. [Online]. Available: http://henke.lbl.gov/optical_constants/atten2.html
- [10] H. Burešová *et al.*, "Preparation and luminescence properties of ZnO: Ga-polystyrene composite scintillator," *Opt. Expr.*, vol. 24, no. 14, pp. 15289–15298, Jul. 2016.
- [11] M. A. Becker *et al.*, "Bright triplet excitons in caesium lead halide perovskites," *Nature*, vol. 553, no. 7687, pp. 189–193, Jan. 2018.
- [12] Q. Chen *et al.*, "All-inorganic perovskite nanocrystal scintillators," *Nature*, vol. 561, no. 7721, pp. 88–93, Sep. 2018.